

**Supporting Information:**  
**Temperature-sensitive Soft Microgels at**  
**Interfaces: Air-Water versus Oil-Water**

Steffen Bochenek, Andrea Scotti, and Walter Richtering\*

*Institute of Physical Chemistry, RWTH Aachen University, Landoltweg 2, 52056 Aachen,  
Germany*

E-mail: richtering@rwth-aachen.de

## $\Pi$ -Area Compression Isotherms.

$\Pi$ -*area/mass* compression isotherms are presented in Figure S1A and B. The trough area was normalized by the initial amount of microgel added to the interface.  $\Pi$ -*area/mass* compression isotherms are subject to the assumption that all microgels adsorb to the interface and there is no loss to the sub-phase. This assumption is discussed in more detail in References.<sup>S1,S2</sup> To avoid this assumption we present  $\Pi$ - $N_{area}$  compression isotherms in the main body, where the  $N_{area}$  is determined from AFM images of deposited monolayers.

Here is a small qualitative difference between the isotherms at the air-water and oil-water interface. In case of decane-water interfaces a sharp transition takes place at the contact point, where the isotherms increase for the first time. For isotherms at the air-water interface this passage is much smoother and further extended. This change is observed at both temperatures (Fig. S1A and B). We attribute the more gradual increase to the stronger stretching of individual microgels within the monolayer. The strongly stretched microgels at first contribute very little to the detectable surface pressure and need to be compressed before a strong increase is registered.

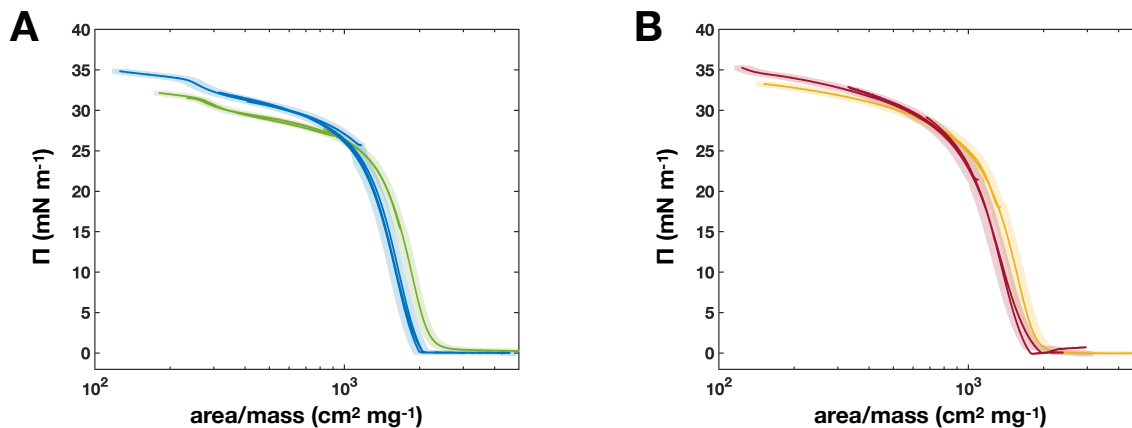


Figure S1: Compression isotherms,  $\Pi$  versus area per mass of microgel added to the interfaces, *area/mass*, of pNIPAM microgels at the air-water and decane-water interface. (A) Comparison of air-water (green) and decane-water (blue) interfaces at  $T = 20^\circ\text{C}$ . (B) Comparison of air-water (gold) and decane-water (red) interfaces at  $T = 40^\circ\text{C}$ . The errors are presented as shaded areas in the respective color.

## $\Pi$ - $\zeta_{2D}$ Compression Isotherms

The isotherms in Figure 3 can be normalized to the generalized area fraction,  $\zeta_{2D}$ . Therefore,  $\zeta_{2D}$  is computed using the following equation:

$$\zeta_{2D} = \frac{N_p \cdot A_{2D}}{A_{image}}, \quad (1)$$

where  $N_p$  is the number of particles per image,  $A_{2D}$  is the mean area of the single microgels from the AFM phase images (Figure 1), and  $A_{image}$  is the area of the AFM image.

$\Pi$ - $\zeta_{2D}$  compression isotherms are presented in Figure S2. At both temperatures and interfaces, microgels get into contact at the same  $\zeta_{2D}$  of  $\approx 1.06$ . However, after the contact, isotherms have transitions between the different regime (II-V) at larger  $\zeta_{2D}$  values.

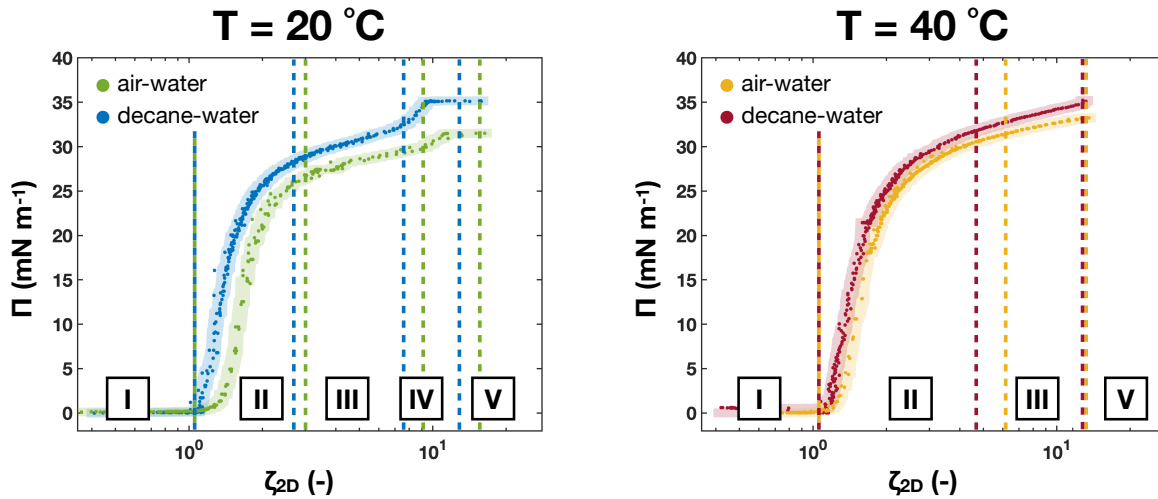


Figure S2:  $\Pi$ - $\zeta_{2D}$  compression isotherms of pNIPAM microgels at the air-water and decane-water interface. (left) Isotherms at  $T = 20\text{ }^\circ\text{C}$ . (right) Isotherms at  $T = 40\text{ }^\circ\text{C}$ . The errors are presented as shaded areas. The different regimes visible in the isotherms are labeled in roman numbers. Dashed lines in the respective colors indicate the transitions.  $\Pi$ -area/mass compression isotherms are presented in the Supporting Information (Fig. S1). Isotherms at oil-water interfaces were adapted with permission from Ref.<sup>S3</sup> Copyright 2020 American Chemical Society.

## AFM Images Before Contact

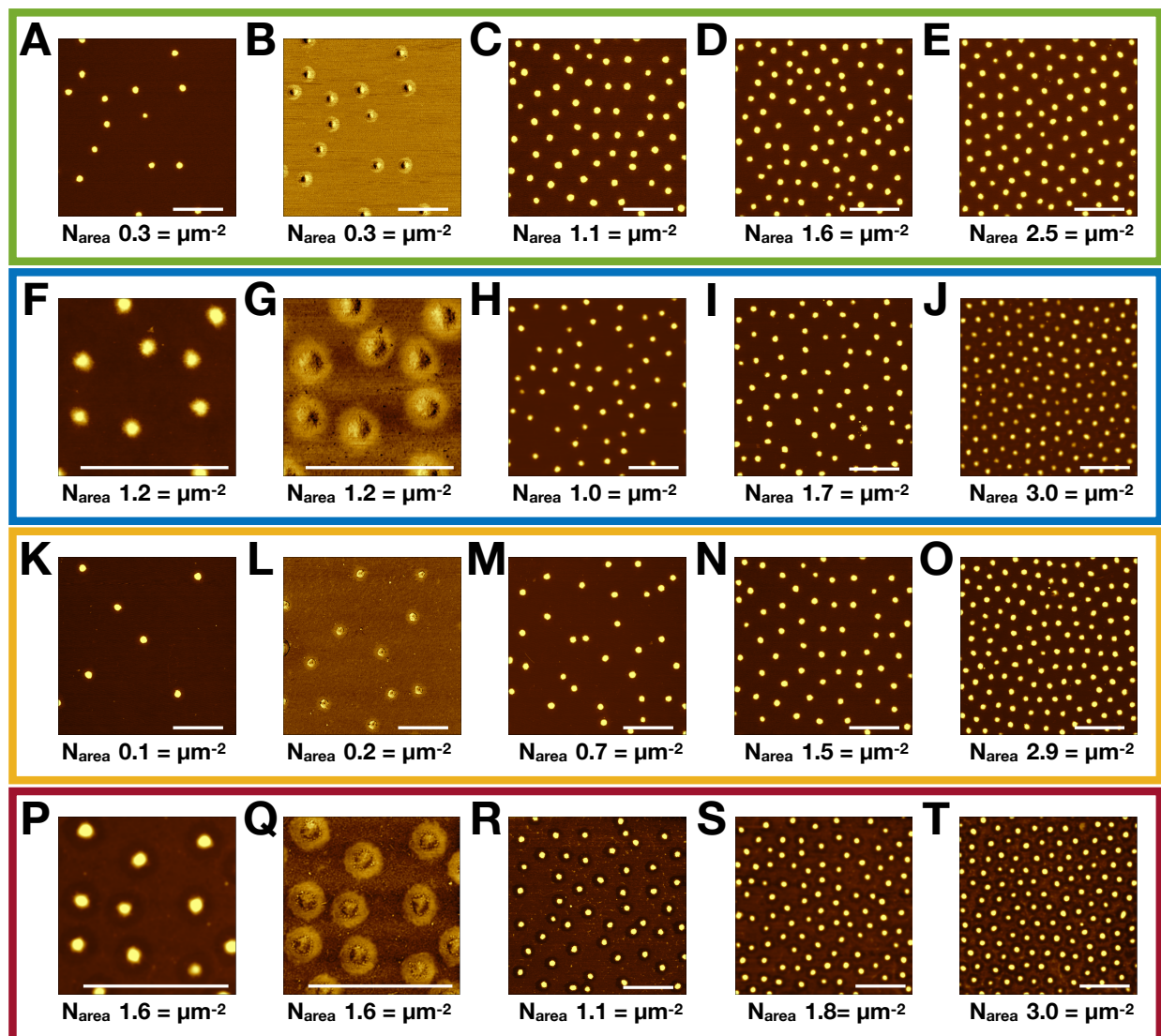


Figure S3: Atomic force micrographs of the microgels before contact deposited at  $T = 20 \text{ }^\circ\text{C}$  from the air-water interface (A-E, green box) and the decane-water interface (F-J, blue box), and deposited at  $40 \text{ }^\circ\text{C}$  from the air-water interface (K-O, golden box) and decane-water interface (P-T, red box) at different compressions. The scale bars are  $2 \mu\text{m}$ .

## Topographic Atomic Force Microscopy

In Table 1 a decrease of  $H_{core}$  is observed for all states (temperature and top-phase) between individual microgels and microgels in contacts. Profiles around  $0.2\text{-}1\text{ mN m}^{-1}$  are about 1 nm lower as the earlier reported profiles of well-separated microgels (Tab. 1). We can relate this reduction to the topographic measurement in the AFM. For a dry, rigid sample, only topographic information are extracted, in contrast to the water-solid interface.<sup>S4</sup> The profiles are relative to the lowest point of the AFM image. At  $\Pi = 0\text{ mN m}^{-1}$ , the microgels are not in contact and the lowest point is the bare substrate. After the contact ( $\Pi \geq 0\text{ mN m}^{-1}$ ), the whole substrate is covered by polymer and  $H_{core}$  is relative to the surface of the microgels' corona. Especially at higher compressions, the disparity of the measured height and real thickness of the dried monolayer is expected to increase, because the microgels are laterally compressed and the unresolved polymer layer becomes thicker.

## Hexagonal Order Parameter.

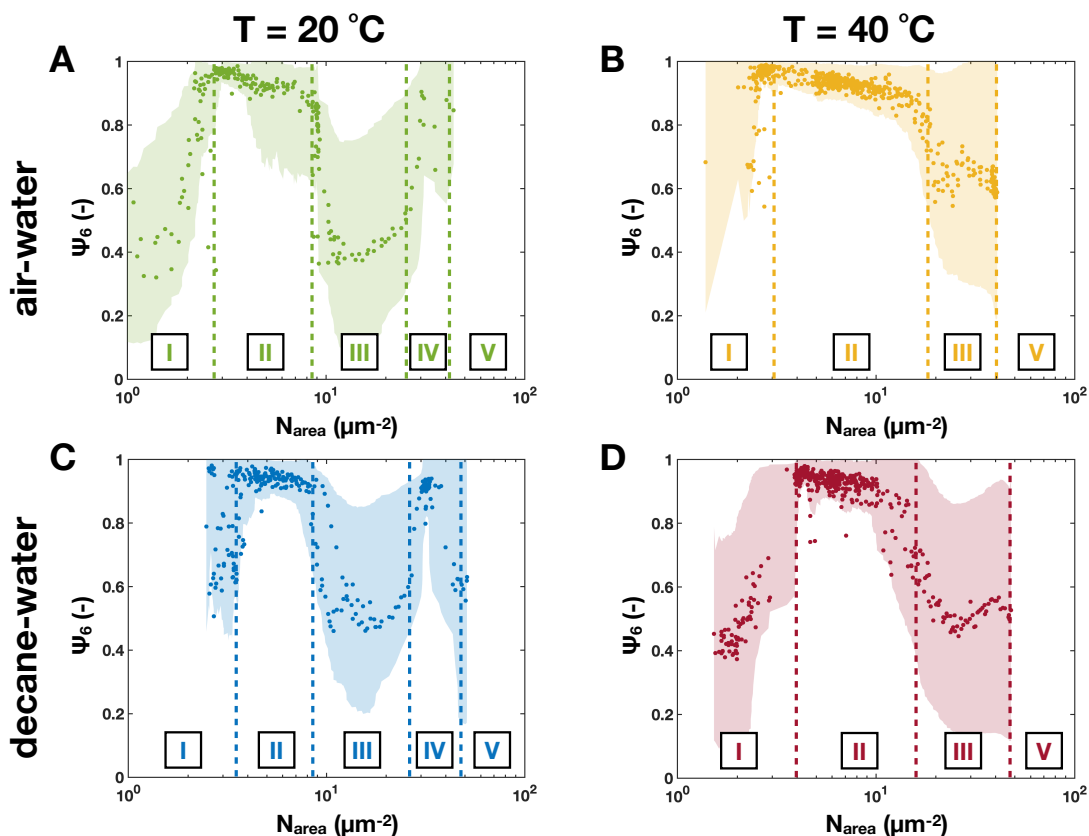


Figure S4: Hexagonal order parameter,  $\Psi_6$ , as a function of number of microgels per area,  $N_{area}$ , of pNIPAM microgels at the air-water and decane-water interface. (A) green full circles:  $T = 20\text{ }^\circ\text{C}$ , air-water interface. (B) golden full circles:  $T = 40\text{ }^\circ\text{C}$ , air-water interface. (C) blue full circles:  $T = 20\text{ }^\circ\text{C}$ , decane-water interface. (D) red full circles:  $T = 40\text{ }^\circ\text{C}$ , decane-water interface. The errors are presented as shaded areas in the respective color. Dashed lines indicate the transitions between different regimes. The regimes are labeled in roman numbers.  $\Psi_6$  versus  $N_{area}$  graphs at oil-water interfaces were adapted with permission from Ref.<sup>S3</sup> Copyright 2020 American Chemical Society.

## References

- (S1) Schmidt, M. M.; Bochenek, S.; Gavrillov, A. A.; Potemkin, I. I.; Richtering, W. Influence of charges on the behavior of polyelectrolyte microgels confined to oil-water interfaces. *Langmuir* **2020**, *36*, 11079–11093.

- (S2) Rey, M.; Fernandez-Rodriguez, M. A.; Steinacher, M.; Scheidegger, L.; Geisel, K.; Richtering, W.; Squires, T. M.; Isa, L. Isostructural solid-solid phase transition in monolayers of soft core-shell particles at fluid interfaces: structure and mechanics. *Soft Matter* **2016**, *12*, 3545–3557.
- (S3) Bochenek, S.; Scotti, A.; Ogieglo, W.; Fernández-Rodríguez, M. A.; Schulte, M. F.; Gumerov, R. A.; Bushuev, N. V.; Potemkin, I. I.; Wessling, M.; Isa, L.; Richtering, W. Effect of the 3D Swelling of Microgels on Their 2D Phase Behavior at the Liquid–Liquid Interface. *Langmuir* **2019**, *35*, 16780–16792.
- (S4) Schulte, M. F.; Scotti, A.; Brugnoli, M.; Bochenek, S.; Mourran, A.; Richtering, W. Tuning the Structure and Properties of Ultra-Low Cross-Linked Temperature-Sensitive Microgels at Interfaces via the Adsorption Pathway. *Langmuir* **2019**, *35*, 14769–14781.